

Nanoscale

Accepted Manuscript



This is an *Accepted Manuscript*, which has been through the Royal Society of Chemistry peer review process and has been accepted for publication.

Accepted Manuscripts are published online shortly after acceptance, before technical editing, formatting and proof reading. Using this free service, authors can make their results available to the community, in citable form, before we publish the edited article. We will replace this *Accepted Manuscript* with the edited and formatted *Advance Article* as soon as it is available.

You can find more information about *Accepted Manuscripts* in the [Information for Authors](#).

Please note that technical editing may introduce minor changes to the text and/or graphics, which may alter content. The journal's standard [Terms & Conditions](#) and the [Ethical guidelines](#) still apply. In no event shall the Royal Society of Chemistry be held responsible for any errors or omissions in this *Accepted Manuscript* or any consequences arising from the use of any information it contains.

demonstrated that a range of layered host compounds can be homogeneously exfoliated into unilamellar 2D crystallites through soft-chemical processes that involve intercalation and swelling of the structures.^{3,19,20} To date, a number of oxide and hydroxide unilamellar nanosheets have been reported. Typical members of this class include $\text{Ti}_{1-x}\text{O}_2^{4x-}$, $\text{MnO}_2^{0.4-}$, $\text{Ca}_2\text{Nb}_3\text{O}_{10}^-$, $\text{Cs}_2\text{W}_{11}\text{O}_{36}^{2-}$, $\text{M}^{2+}_{1-x}\text{M}^{3+}_x(\text{OH})_2^{x+}$ ($\text{M}^{2+} = \text{Mg}^{2+}, \text{Co}^{2+}, \text{Ni}^{2+}, \text{Zn}^{2+}, \dots$, $\text{M}^{3+} = \text{Al}^{3+}, \text{Co}^{3+}, \dots$).³ Because of their considerable diversity with respect to composition and structure, these nanosheets can exhibit a range of physical properties.²¹⁻²² Among these nanosheets, titania nanosheets of $\text{Ti}_{0.91}\text{O}_2^{0.36-}$ and $\text{Ti}_{0.87}\text{O}_2^{0.52-}$ are particularly important because of their versatile functionalities, such as highly efficient absorption of UV light, superior photocatalytic activity and dielectric properties.²⁴⁻²⁸

Intensive research efforts have been devoted to the development of functional nanostructured materials and nanodevices based on 2D nanomaterials.^{3-6,21,22} Precise organization of the 2D crystallites as building blocks has led to a range of advanced functions. In this research direction, the heteroassembly of multiple 2D materials has emerged as a key challenge.^{3,4,21,22,28} The molecularly thin 2D nanosheet structure is ideally suited for being uniformly integrated, which can promote intimate interactions between nanosheets. We can expect the concerted modulation of the physical properties of individual components in such a system, leading to sophisticated functions that cannot be achieved with a single material. In practice, a couple of reports have demonstrated the effectiveness of this strategy. For example, heteroassemblies composed of graphene and transition metal dichalcogenides, typically MoS_2 , or h-BN nanosheets were created as vertically aligned field-effect transistors (FETs), and excellent performance, such as high current density and high on/off ratio, was demonstrated.^{29,30} High photosensitivity was also reported for such heteroassemblies, indicating that these systems have promising applications as highly efficient flexible photovoltaic devices.¹⁸ We have adopted a similar approach for oxide nanosheet systems and demonstrated the evolution of their novel functions: ferroelectricity in the heteroassembly of dielectric nanosheets of $\text{LaNb}_2\text{O}_7/\text{Ca}_2\text{Nb}_3\text{O}_{10}^-$,³¹ photochemical energy conversion in a system composed of semiconducting $\text{Ti}_{0.91}\text{O}_2^{0.36-}$ /redoxable $\text{MnO}_2^{0.4-}$,³² and highly enhanced magneto-optical properties in a superlattice film of ferromagnetic nanosheets of $\text{Ti}_{0.8}\text{Co}_{0.2}\text{O}_2^{0.4-}/\text{Ti}_{0.6}\text{Fe}_{0.4}\text{O}_2^{0.4-}$.³³ Based on these promising results, it would be of significant importance to explore the heterosystem of graphene/oxide nanosheets. For example, if we employ titania nanosheets, new or enhanced electronic functions may be expected due to their photochemical activity and dielectric property. Although there have been a couple of reports on the hybridization of GO and $\text{Ti}_{0.91}\text{O}_2^{0.36-}$ nanosheets, alternating integration at the molecular level was not demonstrated.^{15,34,35} Furthermore, the electrical properties of such a heterosystem have not yet been explored.

In the present study, GO and $\text{Ti}_{0.87}\text{O}_2^{0.52-}$ nanosheets were assembled layer-by-layer to produce nanostructured films. The results of various characterizations indicated that these two types of 2D materials were stacked in an alternating sequence to form a superlattice structure. We observed that GO was effectively reduced into reduced graphene oxide (rGO) under UV light via the photocatalytic action of $\text{Ti}_{0.87}\text{O}_2^{0.52-}$ nanosheets, which may be

due to the molecular-level intimate contact between GO and $\text{Ti}_{0.87}\text{O}_2^{0.52-}$. A FET device was fabricated, employing the resulting rGO/ $\text{Ti}_{0.87}\text{O}_2^{0.52-}$ film as a channel material. The rGO in the film was observed to function as an *n*-type unipolar conductor with significantly enhanced conductivity and electron carrier mobility.

2. Experimental section

Preparation of films by layer-by-layer method and photocatalytic reduction of GO

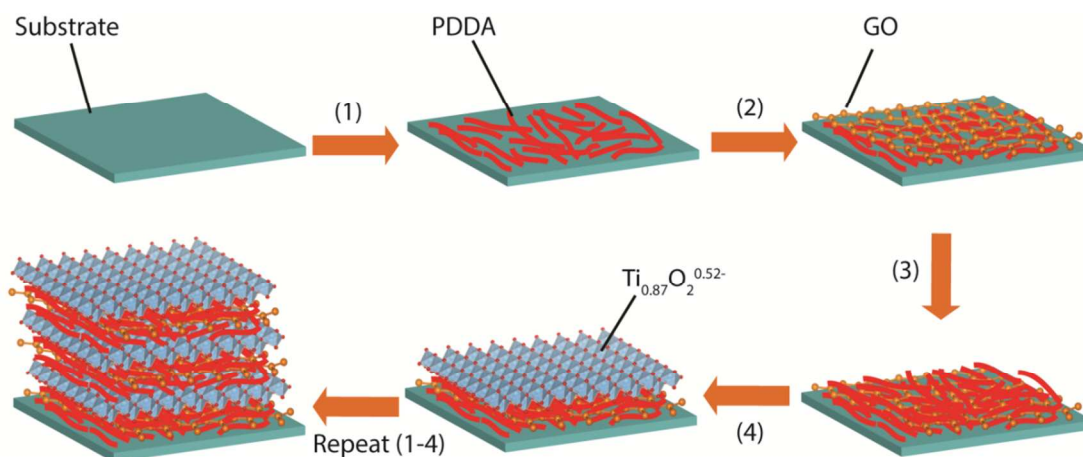
Details of the preparative procedures for GO and titania nanosheets are given in the Electronic Supplementary Information (ESI). GO and $\text{Ti}_{0.87}\text{O}_2^{0.52-}$ nanosheets were adsorbed in various sequences from their colloidal suspensions onto a quartz glass substrate with intermittent dipping into a PDPA solution (20 g dm⁻³, pH = 9). The substrate was immersed in each solution for 20 min, rinsed thoroughly with ultrapure water and dried with a N₂ gas stream. AFM (SPA400, Seiko Instruments Inc.) was used to characterize the coverage of monolayer films on the silicon substrates. UV-visible absorption spectroscopy (SolidSpec-3700 DUV spectrophotometer, Shimadzu) was used to monitor the fabrication of the multilayer films and the GO reduction process upon UV illumination. X-ray photoemission spectra (XPS) (Theta probe Thermo Electron) was employed to examine the GO reduction process. The structural changes in the films before and during the reduction process were characterized by X-ray diffraction (XRD) (Rigaku RINT 2200 powder diffractometer with monochromated Cu K α radiation, $\lambda = 0.15405$ nm). The electrical conductivities of the heterostructured films before and during the photocatalytic reduction were measured by a resistance meter (MCP-HT450, Mitsubishi Chemical Analytech) with a coaxial two-electrode probe.

Device measurements

The electrical transport properties of the (rGO/ $\text{Ti}_{0.87}\text{O}_2^{0.52-}$)₁₀, (rGO)₁₀ and ($\text{Ti}_{0.87}\text{O}_2^{0.52-}$)₁₀ films were examined by fabricating FETs with these films as channel materials on heavily doped Si substrates as gate electrodes. Ti/Au electrodes were fabricated on the film as source and drain terminals *via* EBD. The transistor current-voltage characteristics of the three films were measured under vacuum ($<10^{-3}$ Pa) with a source-to-drain voltage (V_{ds}) of 1 V using a Keithley 4200-SCS parameter analyzer with a low-temperature probe system from Nagase Electronic Equipment Service. The samples were exposed to UV light prior to the measurement to remove adsorbed oxygen molecules.

3. Results and discussion

GO was prepared using the modified Hummers' method,¹⁰ and the $\text{Ti}_{0.87}\text{O}_2^{0.52-}$ nanosheets were produced *via* the soft-chemical exfoliation of a layered titanate, $\text{K}_{0.8}\text{Ti}_{1.73}\text{Li}_{0.27}\text{O}_4$.³⁶ The unilamellar nature of the as-prepared GO and $\text{Ti}_{0.87}\text{O}_2^{0.52-}$ nanosheets was confirmed by atomic force microscopy (AFM) observation (Fig. S1), which indicated that these nanosheets had thicknesses of ~ 0.8 nm and ~ 1.2 nm, respectively. Because GO and $\text{Ti}_{0.87}\text{O}_2^{0.52-}$ are negatively charged, we assembled these nanosheets layer-by-layer using poly(diallyldimethylammonium) (PDPA) chloride as the cationic linker (Scheme 1). Optimizing



Scheme 1 Process for fabricating $(\text{PDDA}/\text{GO}/\text{PDDA}/\text{Ti}_{0.87}\text{O}_2^{0.52-})_n$ superlattice films *via* the layer-by-layer method.

the deposition parameters to attain dense packing of these
 5 nanosheets is of critical importance for constructing well-stacked
 multilayer structures. Because the nanosheet concentration is one
 of the most important deposition parameters, we examined the
 concentration dependence of the surface coverage with GO sheets
 by AFM observations while fixing the other parameters (pH = 9,
 10 deposition time = 20 min). The surface coverage increased as the
 concentration in the suspension increased (Fig. S2-S3). We
 determined that 0.04 g dm^{-3} was optimum for GO, at which the
 coverage reached 90% for the substrate surface, 50% for the
 monolayer region and 40% for the overlapped patches (Fig. 1a).
 15 In contrast, a total coverage of 90% by $\text{Ti}_{0.87}\text{O}_2^{0.52-}$ nanosheets,
 with a monolayer region coverage of 50%, was attained (Fig. 1b)
 at an optimized nanosheet concentration of 0.08 g dm^{-3} ,
 established in our previous study.²⁴

We constructed hetero-assembled films of
 20 $(\text{PDDA}/\text{GO}/\text{PDDA}/\text{Ti}_{0.87}\text{O}_2^{0.52-})_n$ and multilayers of $(\text{PDDA}/\text{GO})_n$
 and $(\text{PDDA}/\text{Ti}_{0.87}\text{O}_2^{0.52-})_n$ by repeating the deposition of each
 nanosheet with PDDA in a designated sequence. Fig. 1c presents
 the AFM image of a film of $\text{PDDA}/\text{GO}/\text{PDDA}/\text{Ti}_{0.87}\text{O}_2^{0.52-}$
 fabricated on a Si substrate, in which smaller $\text{Ti}_{0.87}\text{O}_2^{0.52-}$
 25 nanosheets were resolved on top of larger GO sheets. The
 assembly process on a quartz substrate was monitored using UV-
 visible absorption spectra. GO and $\text{Ti}_{0.87}\text{O}_2^{0.52-}$ exhibited different
 absorption profiles. Enhancement in the absorbance due to GO
 and $\text{Ti}_{0.87}\text{O}_2^{0.52-}$ was observed after each deposition, which
 30 suggests that the target nanostructured films were successfully
 constructed (Fig. 1d and S4). XRD was used to characterize these
 multilayer films. The peaks that appeared at $5\text{-}10^\circ$ result from the
 lamellar structures of the stacked nanosheets (Fig. 1e). The
 intersheet spacings for $(\text{PDDA}/\text{GO})_{10}$ and $(\text{PDDA}/\text{Ti}_{0.87}\text{O}_2^{0.52-})_{10}$
 35 of 1.25 and 1.46 nm, respectively, were similar to those reported
 in the literature.²⁴ The XRD pattern for the
 $(\text{PDDA}/\text{GO}/\text{PDDA}/\text{Ti}_{0.87}\text{O}_2^{0.52-})_5$ films showed a Bragg peak
 centered at $2\theta = 6.5^\circ$, indicating a spacing of 1.35 nm. This value
 coincides with an average intersheet distance of $((1.25+1.46)/2)$
 40 for the two systems composed of each nanosheet and PDDA.
 This result strongly suggests that the observed peak is a second-
 order reflection of a superlattice structure of alternately stacked
 $\text{GO}/\text{Ti}_{0.87}\text{O}_2^{0.52-}$ connected by PDDA (Fig. S5). We calculated the

intensities of the basal reflections based on the supercell model,
 45 obtaining $I_{001}/I_{002}/I_{003} = 8/100/10$ (Fig. S6). The calculated
 intensity of the second-order peak is considerably greater than
 that of the first-order peak, which is consistent with the
 experimental data. These results provide strong support for the
 successful formation of the designed superlattice film of
 50 $\text{Ti}_{0.87}\text{O}_2^{0.52-}$ and GO.

The reduction of GO has been achieved using several different
 processes, typically *via* treatment with a reducing agent such as
 hydrazine, annealing under an inert-gas atmosphere or vacuum,
 and exposure to UV light.^{9,13,15,34,37-42} Although the first two
 55 procedures work well, they have some disadvantages: removal of
 carbon atoms and incompatibility with the electronics industry
 because of the annealing at high temperature,^{37,39} the unstable
 chemical doping, dispersion problem in suspension and use of
 environmentally unfriendly agent such as hydrazine.^{41,42} UV
 60 treatment is generally not efficient.⁴³⁻⁴⁶ In light of these
 disadvantages, photocatalytic reduction may be useful and
 effective because of its gentle, clean and controllable nature.
 However, to date, much less attention has been paid to the
 photocatalytic reduction of GO.

We previously reported that titania nanosheets exhibit efficient
 photocatalytic activity upon UV irradiation to decompose organic
 compounds or to induce superhydrophilicity.^{24,47,48} In the present
 system, photogenerated electrons are expected to transfer from the
 $\text{Ti}_{0.87}\text{O}_2^{0.52-}$ nanosheets to GO, thereby reducing the GO to
 70 remove oxygen-containing functional groups and to restore the
 sp^2 network. Thus, the film of $(\text{PDDA}/\text{GO}/\text{PDDA}/\text{Ti}_{0.87}\text{O}_2^{0.52-})_5$
 fabricated on quartz substrates was exposed to UV light ($\lambda = 270\text{-}$
 400 nm, 2.5 mW cm^{-2}). A controlled UV treatment was
 performed on the $(\text{PDDA}/\text{Ti}_{0.87}\text{O}_2^{0.52-})_{10}$ and $(\text{PDDA}/\text{GO})_5$ films.
 75 Under UV illumination, the color of the hetero-assembled film
 changed from light yellow to brown and finally to dark brown,
 particularly during the first 3 h (Fig. 2a). This color change
 should be attributed to the reduction of GO. The UV-visible
 absorption spectra provide more quantitative information
 80 regarding the color change (Fig. S7). The as-deposited films of
 $(\text{PDDA}/\text{GO}/\text{PDDA}/\text{Ti}_{0.87}\text{O}_2^{0.52-})_5$ and $(\text{PDDA}/\text{Ti}_{0.87}\text{O}_2^{0.52-})_{10}$
 exhibited a sharp absorption band below 300 nm, which is
 primarily due to the $\text{Ti}_{0.87}\text{O}_2^{0.52-}$ nanosheets. Upon UV irradiation,

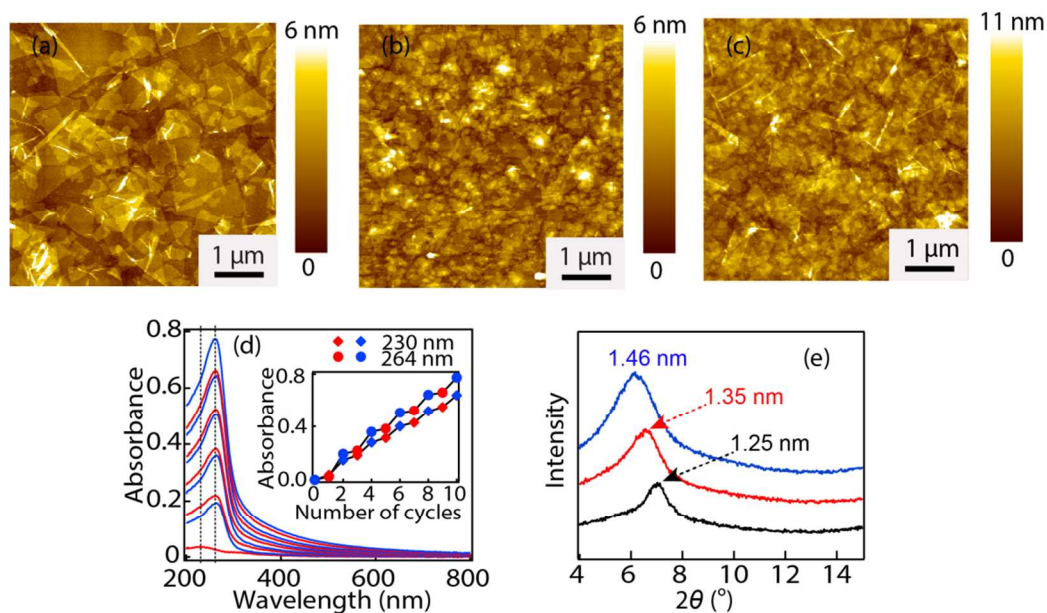


Fig.1 Tapping-mode AFM images of (a) GO deposited from a 0.04 g dm^{-3} suspension onto a Si wafer precoated with PDDA (a), (b) $\text{Ti}_{0.87}\text{O}_2^{0.52-}$ nanosheets deposited from a 0.08 g dm^{-3} suspension and (c) heteroassembly of $\text{GO}/\text{Ti}_{0.87}\text{O}_2^{0.52-}$ connected by PDDA. (d) UV-visible absorption spectra for the assembly process of $(\text{PDDA}/\text{GO}/\text{PDDA}/\text{Ti}_{0.87}\text{O}_2^{0.52-})_5$. (e) XRD patterns for the films of $(\text{PDDA}/\text{Ti}_{0.87}\text{O}_2^{0.52-})_{10}$, $(\text{PDDA}/\text{GO})_{10}$ and $(\text{PDDA}/\text{GO}/\text{PDDA}/\text{Ti}_{0.87}\text{O}_2^{0.52-})_5$ shown as blue, black and red traces, respectively.

the baseline from the hetero-assembled film was noticeably enhanced over the entire spectral range, which is characteristic of metallic materials, whereas the absorption band remained unchanged. This result should be attributed to graphene or rGO, which is known to exhibit a wide absorption band in the wavelength range from 300 nm to $6 \mu\text{m}$.⁷ In contrast, such a change was not observed for the latter film. Our previous study revealed the photocatalytic decomposition of PDDA into NH_4^+/H^+ , which does not bring about color change.²⁵ It is reasonable to assume that both the reduction of GO and the degradation of PDDA occurred in the hetero-assembled film. The resultant NH_4^+/H^+ should act as counter ions to bind rGO and $\text{Ti}_{0.87}\text{O}_2^{0.52-}$ nanosheets. Fig. 2b presents X-ray photoelectron spectra (XPS) of the film before and after the UV treatment. Although quantitative analysis on the degrees of reduction is difficult, it is apparent that the majority of carbon bound to oxygen was reduced by the treatment. As a control, the $(\text{GO}/\text{PDDA})_5$ film was reduced by annealing under vacuum at $400 \text{ }^\circ\text{C}$ for 1 h. The XPS spectrum of the film produced using this standard annealing process is similar to that of the hetero-assembled film after the UV treatment, suggesting that a similar degree of reduction was attained (Table S1).

The optical absorption enhancement in the visible to IR range for $(\text{PDDA}/\text{GO}/\text{PDDA}/\text{Ti}_{0.87}\text{O}_2^{0.52-})_5$ was observed primarily within the first 3 h (Fig. 2c), indicating that the reduction of GO can be rapidly driven to completion. Similar enhancement was also observed for $(\text{PDDA}/\text{GO})_5$ upon UV exposure, suggesting that the reduction of GO only by the UV treatment, as reported in previous studies.⁴³⁻⁴⁶ However, the reduction rate was much slower; the absorbance after 30 h was less than one half that of the hetero-assembled film. It is clear that the photocatalytic reduction of GO with $\text{Ti}_{0.87}\text{O}_2^{0.52-}$ nanosheets is much more efficient.

Changes in the lamellar nanostructures during the process were monitored using XRD. The intersheet spacing of the $(\text{PDDA}/\text{Ti}_{0.87}\text{O}_2^{0.52-})_{10}$ film contracted from 1.46 nm to 0.98 nm over 48 h of UV irradiation (Fig. 2d and S8). This change has been attributed to the photocatalytic decomposition of PDDA into smaller inorganic ions such as NH_4^+ and H^+ .²⁵ The $(\text{PDDA}/\text{GO})_5$ film did not show such a notable contraction, which should be attributed to the absence of the photocatalyst. In the hetero-assembled $(\text{PDDA}/\text{GO}/\text{PDDA}/\text{Ti}_{0.87}\text{O}_2^{0.52-})_5$ film, the primary peak also shifted to a higher angular range, corresponding to a change in d-spacing from 1.35 nm to 0.92 nm (Fig. 2d and S8). Because this peak is the second-order basal reflection from the structure as discussed above (Fig. S5), the net contraction of the unit structure composed of $\text{GO}/\text{Ti}_{0.87}\text{O}_2^{0.52-}$ was $0.86 \text{ nm} (= 2 \times (1.35 - 0.92))$. This value is nearly two times greater than that observed in the $(\text{PDDA}/\text{Ti}_{0.87}\text{O}_2^{0.52-})_{10}$ film, suggesting that the PDDA in the hetero-assembled film would be completely decomposed because the PDDA layer is in contact with the $\text{Ti}_{0.87}\text{O}_2^{0.52-}$ nanosheets. Based on this estimation, the contribution of the reduction of GO to the intersheet contraction may be negligible. Various values for the change in the GO thickness upon reduction have been reported, depending on the treatments and their conditions. Contraction of 0.4-0.5 nm have been frequently observed in the rather powerful chemical or thermal reduction processes, as a result of the removal of functional groups and transition to a hydrophobic nature.^{9,39} These data suggest that the photocatalytic process is milder than the chemical and thermal reduction process. Nevertheless, the sheet resistance of $(\text{PDDA}/\text{GO}/\text{PDDA}/\text{Ti}_{0.87}\text{O}_2^{0.52-})_{10}$ decreased by more than six orders of magnitude (Fig. 2e) during 3 h of UV irradiation, which was comparable to the decrease in resistance achieved through the conventional chemical reduction and annealing methods.^{39-41,49,50} The photocatalytic reduction of GO

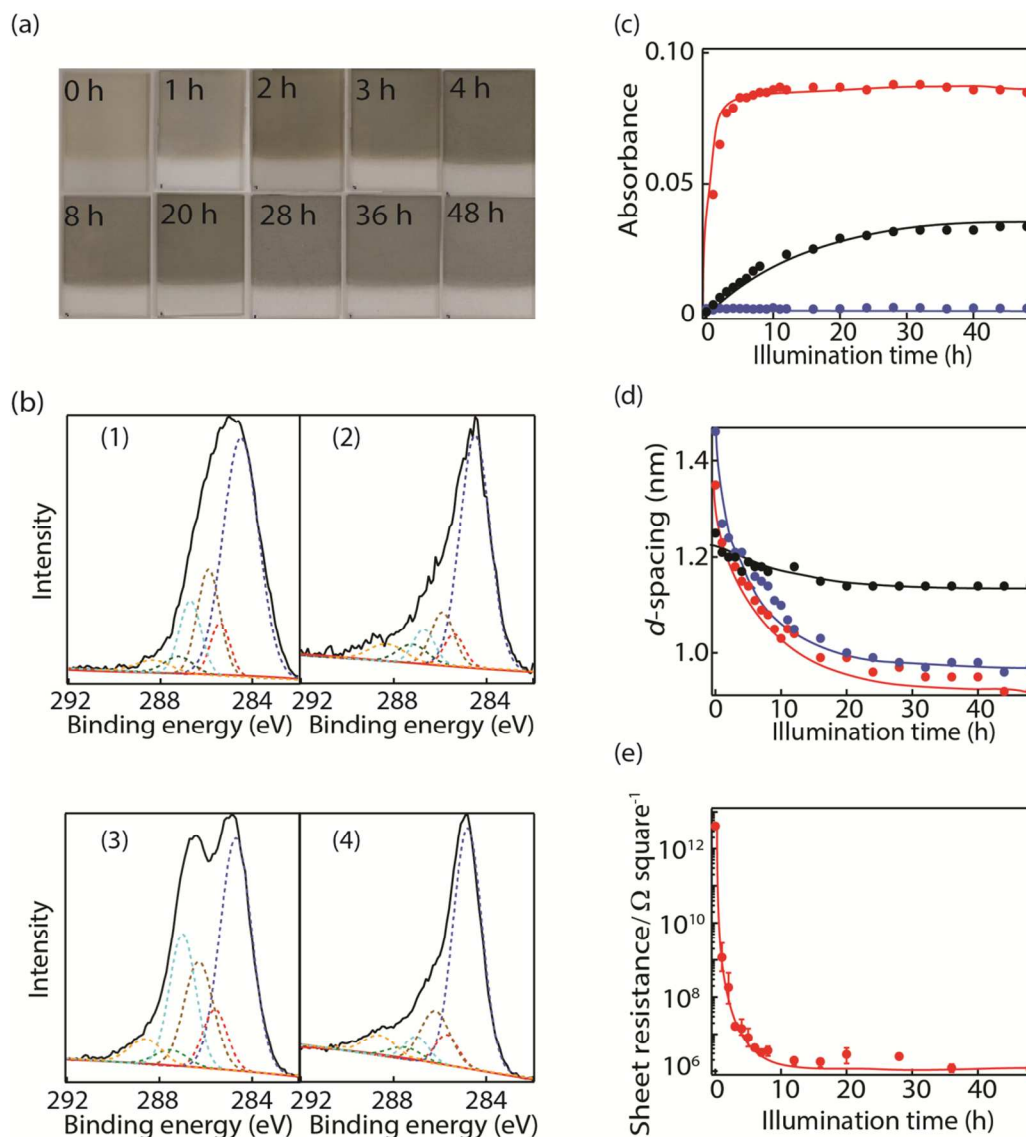


Fig.2 (a) The color change of the (PDDA/GO/PDDA/Ti_{0.87}O₂^{0.52-})₅ film upon UV light illumination ($\lambda = 270\text{-}400\text{ nm}$, approximately 2.5 mW cm^{-2}). (b) High-resolution XPS data for C1s peak: (PDDA/GO/PDDA/Ti_{0.87}O₂^{0.52-})₅ before (1) and after (2) the UV treatment; (PDDA/GO)₅ before (3) and after (4) the thermal reduction process under vacuum at $400\text{ }^{\circ}\text{C}$ for 1 h. The peaks arise from C-C, C=C, C-H (285.0 eV), C-N (285.9 eV), C-OH (286.4 eV), C-O-C (287.2 eV), C=O (287.7 eV) and COO (288.8 eV) are shown as blue, red, brown, light blue, green, and yellow dash traces, respectively. (c) The absorbance at 1300 nm as a function of the UV illumination time for films of (PDDA/Ti_{0.87}O₂^{0.52-})₁₀, (PDDA/GO)₅ and (PDDA/GO/PDDA/Ti_{0.87}O₂^{0.52-})₅ shown as blue, black and red traces, respectively. (d) The change in the basal spacing of the films of (PDDA/Ti_{0.87}O₂^{0.52-})₁₀, (PDDA/GO)₅ and (PDDA/GO/PDDA/Ti_{0.87}O₂^{0.52-})₅ shown as blue, black and red traces, respectively. (e) The change in the sheet resistance of (PDDA/GO/PDDA/Ti_{0.87}O₂^{0.52-})₁₀ film as a function of the UV illumination time.

was investigated using TiO₂ nanoparticles as almost only one example, which reported a limited enhancement (approximately 10 fold) in conductivity.³⁸ The smaller improvement may be due to the fact that dense/homogeneous contact between GO and nanoparticles is difficult to attain. In contrast, in the present system, the GO sheets are in intimate face-to-face contact with the Ti_{0.87}O₂^{0.52-} nanosheets.

In addition to the efficient enhancement in conductivity, the present photocatalytic reduction of GO has other benefits, being free from difficulties for the other processes such as uncontrollable side reactions or undesirable chemical doping. Based on these aspects, this photocatalytic reduction method may

provide a competitive option for applications in electronics.

Subsequently, we fabricated FETs using the resulting (RGO/Ti_{0.87}O₂^{0.52-})₁₀ film as a channel material on a heavily doped Si substrate as a gate electrode, and we expected some intriguing electrical transport properties for the unique superlattice system. The structure of the FET device is illustrated in Fig. 3a. We also fabricated a FET device based on a (rGO)₁₀ film produced using the thermal reduction method. As described above, the XPS data revealed that this process result in the simultaneous reduction of GO and decomposition of PDDA.

Good ohmic contact was observed from the linear current-voltage relationships between the source and drain ($I_{\text{ds}}-V_{\text{ds}}$) for

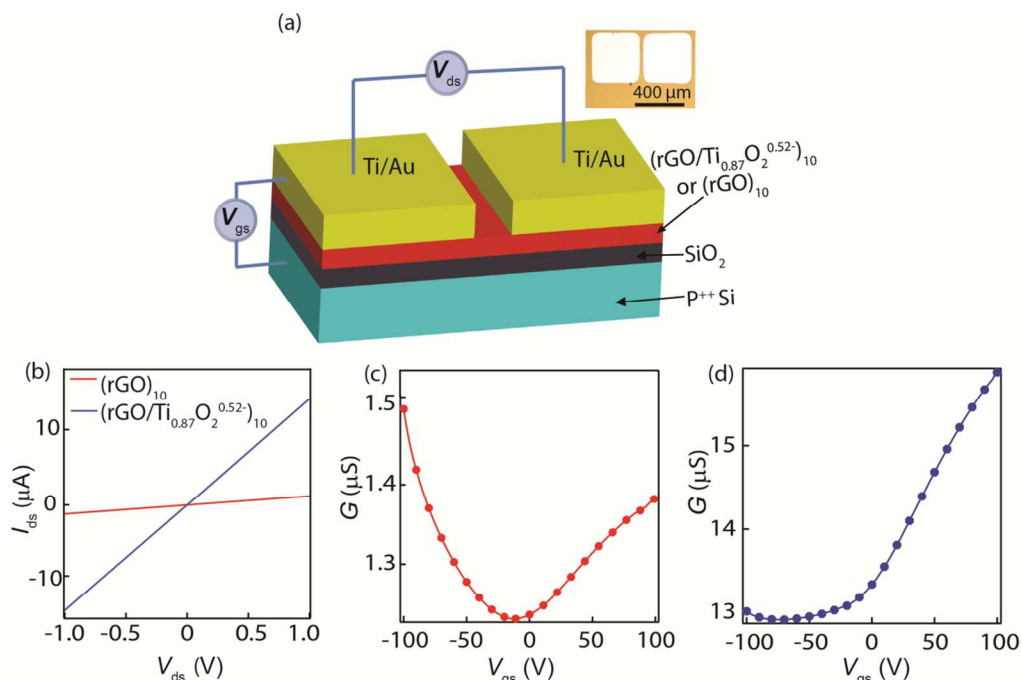


Fig. 3 (a) Schematic diagram of the FET device. (Inset: an optical micrograph of one device, showing two $400 \times 400 \mu\text{m}$ Ti/Au electrodes (channel length: $40 \mu\text{m}$, width: $400 \mu\text{m}$), deposited on the multilayer films by EBD.) (b) $I_{\text{ds}}-V_{\text{ds}}$ curves for $(\text{rGO})_{10}$ and $(\text{rGO}/\text{Ti}_{0.87}\text{O}_2^{0.52-})_{10}$ at $V_{\text{gs}} = 0 \text{ V}$. (c) $G-V_{\text{gs}}$ curves for $(\text{rGO})_{10}$. (d) $G-V_{\text{gs}}$ relationship for the $(\text{rGO}/\text{Ti}_{0.87}\text{O}_2^{0.52-})_{10}$.

the FETs based on both $(\text{rGO}/\text{Ti}_{0.87}\text{O}_2^{0.52-})_{10}$ and $(\text{rGO})_{10}$ (Fig. 3b). Their resistances were 7.7×10^4 and $8.3 \times 10^5 \Omega$, respectively (Fig. 3b), which could be converted into sheet resistances of 7.7×10^5 and $8.3 \times 10^6 \Omega \text{ square}^{-1}$. The value for $(\text{rGO}/\text{Ti}_{0.87}\text{O}_2^{0.52-})_{10}$ is very close to that obtained using the coaxial two electrodes probe (Fig. 2e), which indicates that the influence of the contact resistance between the electrodes and the channel materials in this system is negligible. The conductivity of rGO in the hetero-assembled film was more than one order of magnitude greater than that of the rGO obtained by thermal annealing. Based on the conductance–gate voltage ($G-V$) curves (Fig. 3c and d), the electron carrier mobility for the $(\text{rGO})_{10}$ and $(\text{rGO}/\text{Ti}_{0.87}\text{O}_2^{0.52-})_{10}$ was determined to be 0.017 and $0.227 \text{ cm}^2 \text{ V}^{-1} \text{ s}^{-1}$, respectively. This result reflects the advantageous aspects of rGO produced using the photocatalytic reduction process with $\text{Ti}_{0.87}\text{O}_2^{0.52-}$ nanosheets.

The conductive polarity of the FET based on the $(\text{rGO}/\text{Ti}_{0.87}\text{O}_2^{0.52-})_{10}$ film was unipolar, which is in contrast to the ambipolar conductive polarity for the FET based on rGO only (Fig. 3c and d). Because $\text{Ti}_{0.87}\text{O}_2^{0.52-}$ nanosheets are highly insulating (Fig. S9), the electron conducting behavior in the hetero-assembled film should be governed by the rGO layers. Notably, the majority of the rGO-based materials reported are ambipolar conductors or unipolar p -type conductors,^{12,13,39,40,50-56} but the $(\text{rGO}/\text{Ti}_{0.87}\text{O}_2^{0.52-})_{10}$ in this work produced via photocatalytic reduction is an n -type conductor. This result indicates that only electrons induced in the $\text{Ti}_{0.87}\text{O}_2^{0.52-}$ nanosheets can be injected into rGO and that the holes are immobile, being trapped in the nanosheets. Electron injection to rGO has been reported for several channel systems coupled with various titania materials. This behavior has been understood in

terms of the more negative position of the conduction-band edge of titania materials than that of rGO.^{38,57} Conversely, there may be several possible explanations for the fact that holes cannot be doped from $\text{Ti}_{0.87}\text{O}_2^{0.52-}$ nanosheets to rGO, such as more positive valence-band edge of rGO or the presence of hole scavengers in the vicinity of $\text{Ti}_{0.87}\text{O}_2^{0.52-}$ nanosheets. A clear conclusion awaits further in-depth investigation.

The temperature-dependences of the transport properties were measured to gain insights into the charge transport mechanism in the $(\text{rGO})_{10}$ and $(\text{rGO}/\text{Ti}_{0.87}\text{O}_2^{0.52-})_{10}$ films (Fig. 4a and b). As the temperature decreased, the conductance significantly decreased and the on/off ratio slightly increased (Fig. S10). A similar behavior has been observed in GO-based composites and individual GO layers.^{12,52}

Changes of $\ln(G_{\text{min}})$ as functions of $T^{-1/3}$ are plotted in Fig. 4c. The data from both $(\text{rGO}/\text{Ti}_{0.87}\text{O}_2^{0.52-})_{10}$ and $(\text{rGO})_{10}$ films can be fitted linearly to the 2D variable range hopping (VRH) model, suggesting a major contribution of carrier hopping in and between the rGOs to the conductance.^{12,51,53} The fitted slopes are slightly different between the higher and lower temperature regions, particularly for the $(\text{rGO}/\text{Ti}_{0.87}\text{O}_2^{0.52-})_{10}$ film. It has been reported that thermal activation of charge carriers also contributes to the temperature dependence of the conductivity in rGO.^{12,51} As described in the following section, we expect that the conductivity in the higher temperature regions is particularly enhanced by the thermal activation of carrier mobility and concentration, and such an effect of the excitation is more pronounced in the $(\text{rGO}/\text{Ti}_{0.87}\text{O}_2^{0.52-})_{10}$ film than the $(\text{rGO})_{10}$.

The channel material of $(\text{rGO}/\text{Ti}_{0.87}\text{O}_2^{0.52-})_{10}$ is composed of alternately stacked rGO and $\text{Ti}_{0.87}\text{O}_2^{0.52-}$ micron-sized nanosheets. As shown in Fig. 1, each layer of GO and $\text{Ti}_{0.87}\text{O}_2^{0.52-}$ consists of

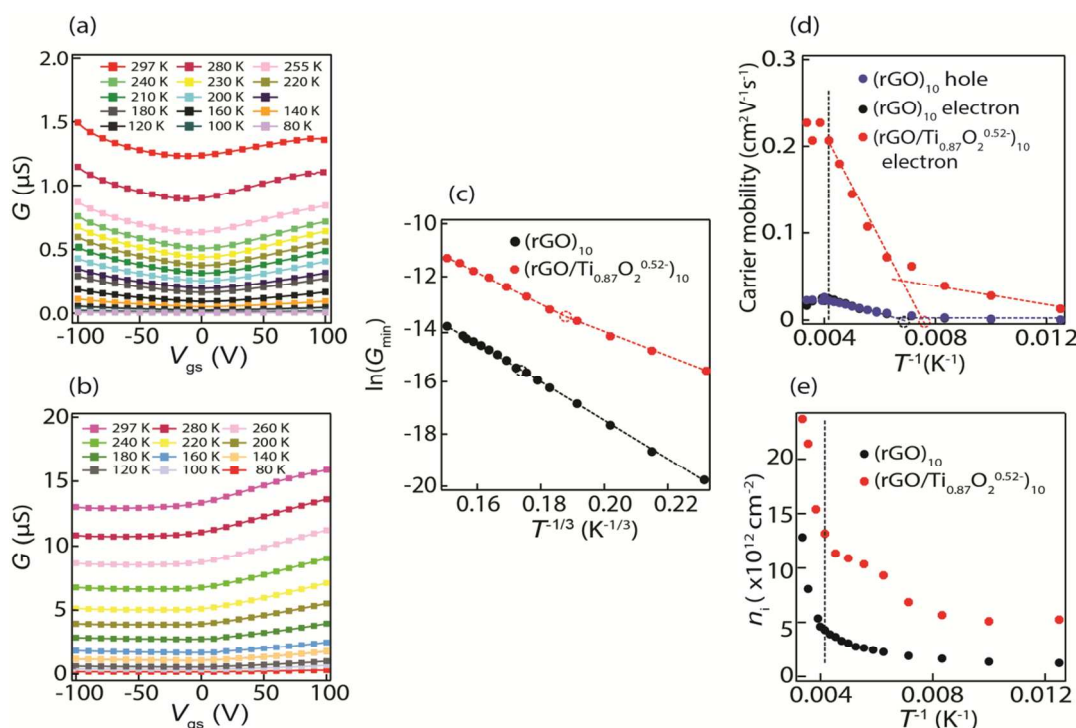


Fig. 4 Temperature-dependent G - V curves for the films of (rGO)₁₀ (a) and (rGO/Ti_{0.87}O₂^{0.52-})₁₀ (b). (c) $\ln(G_{\min})$ as functions of $T^{-1/3}$ for (rGO/Ti_{0.87}O₂^{0.52-})₁₀ and (rGO)₁₀ films. (d) The carrier mobility as a function of the reciprocal of the temperature. (e) The intrinsic electron carrier concentration as a function of the reciprocal of the temperature.

many 2D nanosheets that possess overlaps and gaps between them. This indicates that the GO layer as a conduction path has many boundaries, and the carriers move within and between different rGO sheets. The temperature dependence of the carrier mobility is depicted as a function of T^{-1} , showing the inflection points (broken-line circles) in Fig. 4d, which roughly correspond to those in Fig. 4c. The carrier mobility exhibits considerably larger temperature dependence and enhanced values in the range above the transition points. The increase in carrier mobility is larger for (rGO/Ti_{0.87}O₂^{0.52-})₁₀ than for (rGO)₁₀, suggesting that the carrier transport in rGO nanosheets is activated more easily in those produced *via* photocatalytic reduction with Ti_{0.87}O₂^{0.52-} nanosheets (Fig. 4d). This behavior is likely due to the reduced energy barriers for carriers transferring between the rGO sheets being sandwiched with Ti_{0.87}O₂^{0.52-} nanosheets that have a very high dielectric constant. In addition to this dielectric shielding effect, the better in-plane structure of rGO produced *via* photocatalytic reduction with Ti_{0.87}O₂^{0.52-} nanosheets may also contribute to it to some extent. When the temperature exceeded the transition at 240 K, the carrier concentration also significantly increased (Fig. 4e), most likely due to the activation of carriers from defects and doping states,¹² contributing to the substantial increase in conductance at temperatures above 240 K.

4. Conclusions

Genuine superlattice films of GO/Ti_{0.87}O₂^{0.52-} have been successfully fabricated through the solution-based layer-by-layer assembly technique. UV irradiation effectively activated the photocatalytic reduction of GO sheets within a few hours. The

sheet resistance of the film was decreased by six orders of magnitude in this process. This photocatalytic reduction of GO sheets is competitive with the well-studied chemical or thermal reduction methods in terms of its limited side effects. The in-depth examination of the transport properties of FET devices fabricated with the superlattice rGO/Ti_{0.87}O₂^{0.52-} film as a channel material revealed that the rGO sheets in the film function as a unipolar n -type conductor. Significant improvements in the conductivity and electron carrier mobility of the rGO film by more than one order of magnitude were attained as a result of the heteroassembly with photocatalytic and dielectric oxide nanosheets at the molecular level.

Acknowledgments

This work was partly supported by the World Premier International Research Center Initiative on Materials Nanoarchitectonics (WPI-MANA), MEXT, Japan, and by CREST of the Japan Science and Technology Agency (JST). K. Ohno, W. Tian and S. -L. Li in NIMS helped with the FET property measurements, and K. Tamura helped with the EBD.

Notes and references

- 1 A. K. Geim, *Science* 2009, **324**, 1530.
- 2 M. Xu, T. Liang, M. Shi, H. Chen, *Chem. Rev.* 2013, **113**, 3766.
- 3 R. Ma, T. Sasaki, *Adv. Mater.* 2010, **22**, 5082.
- 4 A. K. Geim, I. V. Grigorieva, *Nature* 2013, **499**, 419.
- 5 I. Meric, M. Y. Han, A. F. Young, B. Ozyilmaz, P. Kim, K. L. Shepard, *Nat. Nanotechnol.* 2008, **3**, 654.
- 6 K. S. Novoselov, A. K. Geim, S. V. Morozov, D. Jiang, Y. Zhang, S. V. Dubonos, I. V. Grigorieva, A. A. Firsov, *Science* 2004, **306**, 666.

- 7 Y. Liu, R. Cheng, L. Liao, H. Zhou, J. Bai, G. Liu, L. Liu, Y. Huang, X. Duan, *Nat. Commun.* 2011, **2**, 579.
- 8 S.-L. Li, H. Miyazaki, A. Kumatani, A. Kanda, K. Tsukagoshi, *Nano Lett.* 2010, **10**, 2357.
- 9 S. Stankovich, D. A. Dikin, R. D. Piner, K. A. Kohlhaas, A. Kleinhammes, Y. Jia, Y. Wu, S. T. Nguyen, R. S. Ruoff, *Carbon* 2007, **45**, 1558.
- 10 W. S. Hummers, R. E. Offeman, *J. Am. Chem. Soc.* 1958, **80**, 1339.
- 11 S. Stankovich, D. A. Dikin, G. H. B. Dommett, K. M. Kohlhaas, E. J. Zimney, E. A. Stach, R. D. Piner, S. T. Nguyen, R. S. Ruoff, *Nature* 2006, **442**, 282.
- 12 G. Eda, M. Chhowalla, *Nano Lett.* 2009, **9**, 814.
- 13 G. Eda, G. Fanchini, M. Chhowalla, *Nat. Nanotechnol.* 2008, **3**, 270.
- 14 C. Mattevi, G. Eda, S. Agnoli, S. Miller, K. A. Mkhoyan, O. Celik, D. Mastrogiovanni, G. Granozzi, E. Garfunkel, M. Chhowalla, *Adv. Funct. Mater.* 2009, **19**, 2577.
- 15 K. K. Manga, Y. Zhou, Y. Yan, K. P. Loh, *Adv. Funct. Mater.* 2009, **19**, 3638.
- 16 B. Radisavljevic, A. Radenovic, J. Brivio, V. Giacometti, A. Kis, *Nat. Nanotechnol.* 2011, **6**, 147.
- 17 C. R. Dean, A. F. Young, I. Meric, C. Lee, L. Wang, S. Sorgenfrei, K. Watanabe, T. Taniguchi, P. Kim, K. L. Shepard, J. Hone, *Nat. Nanotechnol.* 2010, **5**, 722.
- 18 L. Britnell, R. M. Ribeiro, A. Eckmann, R. Jalil, B. D. Belle, A. Mishchenko, Y.-J. Kim, R. V. Gorbachev, T. Georgiou, S. V. Morozov, A. N. Grigorenko, A. K. Geim, C. Casiraghi, A. H. C. Neto, K. S. Novoselov, *Science* 2013, **340**, 1311.
- 19 H.-N. Kim, S. W. Keller, T. E. Mallouk, J. Schmitt, G. Decher, *Chem. Mater.* 1997, **9**, 1414.
- 20 T. Sasaki, M. Watanabe, H. Hashizume, H. Yamada, H. Nakazawa, *J. Am. Chem. Soc.* 1996, **118**, 8329.
- 21 M. Osada, T. Sasaki, *Adv. Mater.* 2012, **24**, 210.
- 22 M. Osada, T. Sasaki, *J. Mater. Chem.* 2009, **19**, 2503.
- 23 The charge of the nanosheets comes from the stoichiometry of the starting layered titanates, $\text{Cs}_{0.7}\text{H}_{1.825}\text{O}_4$ and $\text{K}_{0.8}\text{H}_{1.73}\text{Li}_{0.27}\text{O}_4$. They were converted into acid-exchanged phases with compositions of $\text{H}_{0.7}\text{Ti}_{1.825}\text{O}_4 \cdot \text{H}_2\text{O}$ and $\text{H}_{1.07}\text{Ti}_{1.73}\text{O}_4 \cdot \text{H}_2\text{O}$, respectively, and then delaminated with a TBA solution into the nanosheets of $\text{Ti}_{0.91}\text{O}_2^{0.36}$ and $\text{Ti}_{0.87}\text{O}_2^{0.52}$.
- 24 T. Sasaki, Y. Ebina, T. Tanaka, M. Harada, M. Watanabe, G. Decher, *Chem. Mater.* 2001, **13**, 4661.
- 25 T. Sasaki, Y. Ebina, K. Fukuda, T. Tanaka, M. Harada, M. Watanabe, *Chem. Mater.* 2002, **14**, 3524.
- 26 T. Sasaki, Y. Ebina, M. Watanabe, G. Decher, *Chem. Commun.* 2000, 2163.
- 27 M. Osada, Y. Ebina, H. Funakubo, S. Yokoyama, T. Kiguchi, K. Takada, T. Sasaki, *Adv. Mater.* 2006, **18**, 1023.
- 28 L. Wang, T. Sasaki, *Chem. Rev.* 2014, DOI 10.1021/cr400627u.
- 29 L. Britnell, R. V. Gorbachev, R. Jalil, B. D. Belle, F. Schedin, A. Mishchenko, T. Georgiou, M. I. Katsnelson, L. Eaves, S. V. Morozov, N. M. R. Peres, J. Leist, A. K. Geim, K. S. Novoselov, L. A. Ponomarenko, *Science* 2012, **335**, 947.
- 30 W. J. Yu, Z. Li, H. Zhou, Y. Chen, Y. Wang, Y. Huang, X. Duan, *Nat. Mater.* 2013, **12**, 246.
- 31 B.-W. Li, M. Osada, T. C. Ozawa, Y. Ebina, K. Akatsuka, R. Ma, H. Funakubo, T. Sasaki, *ACS Nano* 2010, **4**, 6673.
- 32 N. Sakai, K. Fukuda, Y. Omomo, Y. Ebina, K. Takada, T. Sasaki, *J. Phys. Chem. C* 2008, **112**, 5197.
- 33 M. Osada, Y. Ebina, K. Takada, T. Sasaki, *Adv. Mater.* 2006, **18**, 295.
- 34 W. Tu, Y. Zhou, Q. Liu, Z. Tian, J. Gao, X. Chen, H. Zhang, J. Liu, Z. Zou, *Adv. Funct. Mater.* 2012, **22**, 1215.
- 35 N. Yang, Y. Zhang, J. E. Halpert, J. Zhai, D. Wang, L. Jiang, *Small* 2012, **8**, 1762.
- 36 T. Sasaki, F. Kooli, M. Iida, Y. Michiue, S. Takenouchi, Y. Yajima, F. Izumi, B. C. Chakoumakos, M. Watanabe, *Chem. Mater.* 1998, **10**, 4123.
- 37 A. Bagri, C. Mattevi, M. Acik, Y. J. Chabal, M. Chhowalla, V. B. Shenoy, *Nat. Chem.* 2010, **2**, 581.
- 38 G. Williams, B. Seger, P. V. Kamat, *ACS Nano* 2008, **2**, 1487.
- 39 V. C. Tung, M. J. Allen, Y. Yang, R. B. Kaner, *Nat. Nanotechnol.* 2009, **4**, 25.
- 40 G. Eda, M. Chhowalla, *Adv. Mater.* 2010, **22**, 2392.
- 41 D. Li, M. B. Muller, S. Gilje, R. B. Kaner, G. G. Wallace, *Nat. Nanotechnol.* 2008, **3**, 101.
- 42 S. Park, J. An, I. Jung, R. D. Piner, S. J. An, X. Li, A. Velamakanni, R. S. Ruoff, *Nano Lett.* 2009, **9**, 1593.
- 43 M. P. McDonald, A. Eltom, F. Vietmeyer, J. Thapa, Y. V. Morozov, D. A. Sokolov, J. H. Hodak, K. Vinodgopal, P. V. Kamat, M. Kuno, *Nano Lett.* 2013, **13**, 5777.
- 44 M. Koinuma, C. Ogata, Y. Kamei, K. Hatakeyama, H. Tateishi, Y. Watanabe, T. Taniguchi, K. Gezuhara, S. Hayami, A. Funatsu, M. Sakata, Y. Kuwahara, S. Kurihara, Y. Matsumoto, *J. Phys. Chem. C* 2012, **116**, 19822.
- 45 Y. H. Ding, P. Zhang, Q. Zhuo, H. M. Ren, Z. M. Yang, Y. Jiang, *Nanotechnology* 2011, **22**, 215601.
- 46 Y. Matsumoto, M. Koinuma, S. Y. Kim, Y. Watanabe, T. Taniguchi, K. Hatakeyama, H. Tateishi, S. Ida, *ACS Appl. Mater. Interfaces* 2010, **2**, 3461.
- 47 T. Shibata, N. Sakai, K. Fukuda, Y. Ebina, T. Sasaki, *Phys. Chem. Chem. Phys.* 2007, **9**, 2413.
- 48 N. Sakai, K. Fukuda, T. Shibata, Y. Ebina, K. Takada, T. Sasaki, *J. Phys. Chem. B* 2006, **110**, 6198.
- 49 Z. Xu, Y. Bando, L. Liu, W. Wang, X. Bai, D. Golberg, *ACS Nano* 2011, **5**, 4401.
- 50 I. Jung, D. A. Dikin, R. D. Piner, R. S. Ruoff, *Nano Lett.* 2008, **8**, 4283.
- 51 J. T. Han, B. J. Kim, B. G. Kim, J. S. Kim, B. H. Jeong, S. Y. Jeong, H. J. Jeong, J. H. Cho, G.-W. Lee, *ACS Nano* 2011, **5**, 8884.
- 52 C. Gómez-Navarro, R. T. Weitz, A. M. Bittner, M. Scolari, A. Mews, M. Burghard, K. Kern, *Nano Lett.* 2007, **7**, 3499.
- 53 A. B. Kaiser, C. Gómez-Navarro, R. S. Sundaram, M. Burghard, K. Kern, *Nano Lett.* 2009, **9**, 1787.
- 54 H. Feng, R. Cheng, X. Zhao, X. Duan, J. Li, *Nat. Commun.* 2013, **4**, 1539.
- 55 T. Kobayashi, N. Kimura, J. Chi, S. Hirata, D. Hobar, *Small* 2010, **6**, 1210.
- 56 J. Yang, J.-W. Kim, H. S. Shin, *Adv. Mater.* 2012, **24**, 2299.
- 57 Y.-B. Tang, C.-S. Lee, J. Xu, Z.-T. Liu, Z.-H. Chen, Z. He, Y.-L. Cao, G. Yuan, H. Song, L. Chen, L. Luo, H.-M. Cheng, W.-J. Zhang, I. Bello, S.-T. Lee, *ACS Nano* 2010, **4**, 3482.